J. Phys. B: At. Mol. Opt. Phys. **23** (1990) 4005–4018. Printed in the UK

Cross-check of elastic differential cross sections and measurement of excitation and ionization cross sections for electron–mercury scattering

F J Peitzmann and J Kessler

Physikalisches Institut der Universität Münster, D-4400 Münster, Federal Republic of Germany

Received 25 April 1990, in final form 13 July 1990

Abstract. Absolute differential and angle-integrated cross sections for elastic electron scattering from mercury were measured at 100, 150 and 300 eV to check the internal consistency of two data sets obtained with a static gas target and an atomic beam. In addition, absolute differential and angle-integrated cross sections for excitation and ionization were obtained. The scattering angles range from 1° (2° at 100 eV) to 165°. An atomic beam target with a diameter small compared with the acceptance angle of the detecting system was used. Because of the difficulty in determining the absolute target density, only relative cross sections were measured. However, integration yielded a total cross section which was normalized to an absolutely measured one. Using the normalization factor thus obtained, the relative cross sections were brought to an absolute scale. The two methods usually agree to within an uncertainty of ±16% of the present measurement.

1. Introduction

Absolute differential cross sections for elastic electron scattering from mercury have previously been measured with a static gas target by Bromberg (1969) and Holtkamp et al (1987). This method yields absolute values by measuring the ratio of the scattered and primary currents and the target density, but one has to rely on a calculation of the effective scattering path length (Silverstein 1959). This path length changes with the scattering angle, a variation which can be compensated by a 'sine correction' factor provided that the primary electron beam and the scattered electrons travel through completely field-free regions warranting straight trajectories. At small scattering angles especially this correction becomes delicate (e.g. at 2° the correction factor becomes approximately 30) and the sensitivity of the method to residual stray fields is greatly increased.

In the past few years the method of the static gas target has been used in our laboratory for absolute cross section measurements (e.g. Holtkamp *et al* 1987, Peitzmann and Kessler 1990). Despite our careful analysis of the method and its systematic errors we felt it worthwhile to cross-check the results by a completely different method. We used a crossed beam technique where the complications mentioned above can be avoided when the scattering volume is totally embedded in the acceptance cone of the detection system (Shyn *et al* 1972). If this condition is fulfilled (which is checked as

0953-4075/90/214005+14$03.50

described in section 2), the scattering volume, within the experimental error limits, does not depend on the scattering angle and need not be known if, as a first step, only relative differential cross sections are measured. To place the values thus obtained on an absolute scale we normalized them to the absolute total cross section measured by Ohnemus and Jost (1979). We chose the energy range from 100 to 300 eV as an overlap with Holtkamp *et al* (1987) because in this region problems of the present method due to adjustment and stray fields are minimized. Thus it became possible to verify the results obtained with the the static gas target method. In addition, our measurements provide absolute values for differential excitation and ionization cross sections which have hitherto not been available.

2. Experimental method

The set-up is shown schematically in figure 1. The primary electron beam is rotatable about the axis of the atomic beam. The horizontal scattering plane is defined by the electron beam and the axis of the stationary detector. This axis and the primary beam axis aim at the centre of the atomic beam. The scattering volume is defined by the intersection of the two beams. Considerable effort has been made to adjust the apparatus carefully. The scattering volume must be located within the acceptance cone of the filter lens so that no 'sine correction' has to be applied. On the other hand, the acceptance cone should not be too large if background scattering is to be negligible. Both conditions were fulfilled by using a suitable aperture system (see section 3) and were checked by swivelling the filter lens before a new measurement was started. In the region where this did not change the measured current (the 'plateau' sketched in figure 1) the atomic beam had a proper position. Scattering by the background gas is most important at small scattering angles because then the primary electron beam travels a long way within the acceptance cone of the filter lens. In order to check this influence, the scattered current was measured with the mercury oven far away from the scattering centre. It was found that background scattering contributed less than 1% at any scattering angle. Therefore no correction was applied (Fink *et al* 1975).

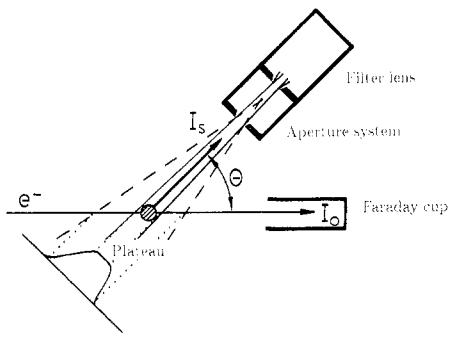

Figure 1. Schematic diagram of the experiment. The atomic beam is denoted by a hatched circle. The transmission of the aperture system is indicated.

The current I_{ela} of electrons scattered elastically by the atomic beam through an angle θ is

$$I_{ela}(\theta) = I_0\,\sigma_{ela}(\theta)\,\Delta\Omega \int n(l)\,dl \qquad (1)$$

where $\Delta\Omega$ is the solid angle subtended by the detector, I_0 the primary current, $\sigma_{ela}(\theta)$ the elastic differential cross section, n the number density of the atomic beam and l the scattering path length. Although the product $c = \Delta\Omega \int n(l)\,dl$ is constant at all scattering angles the quantity $\sigma_{ela}(\theta)$ could not be determined from (1) because it is not easy to obtain the number density of the atomic beam. A measurement of $I_{ela}(\theta)/I_0$ does, however, yield relative values of $\sigma_{ela}(\theta)$. These values have been placed on an absolute scale by normalization to the absolute total cross section Q_{tot} which was measured by Ohnemus and Jost (1979) and which is defined by

$$Q_{tot} = \iint [\sigma_{ela}(\theta) + \sigma_{exci}(\theta) + \sigma_{ion}(\theta)] \sin\theta \, d\theta \, d\phi \tag{2}$$

where $\sigma_{exci}(\theta)$ and $\sigma_{ion}(\theta)$ denote the differential cross sections of all excitation and ionization processes, respectively. In order to determine $\sigma_{exci}(\theta)$ and $\sigma_{ion}(\theta)$, the electrons that have excited or ionized the mercury atom were detected with a filter lens. In a similar way to (1) the corresponding currents are given by

$$\frac{I_{exci}(\theta)}{I_0} = c\sigma_{exci}(\theta) \qquad \frac{I_{ion}(\theta)}{I_0} = c\sigma_{ion}(\theta). \tag{3}$$

With (1) to (3) we obtain

$$Q_{tot} = \frac{2\pi}{c} \int \frac{I_{tot}}{I_0} \sin\theta \, d\theta \tag{4}$$

with $I_{tot} = I_{ela} + I_{exci} + I_{ion}$. The primary current I_0 is kept in the integral because in our experiment it depends slightly on θ, presumably due to residual magnetic fields.

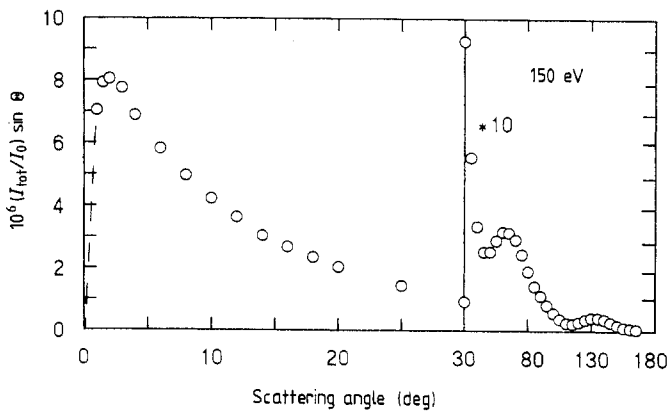

Figure 2. An example of the measurement of $(I_{tot}/I_0)\sin\theta$ versus θ at 150 eV primary energy. In the range from 30° to 180° the abscissa is squeezed and the ordinate is stretched by a factor of 10 so that the areas under the curves can be compared directly. The extrapolation for $\theta \to 0°$ at the angles not covered by the measurement is indicated by the broken curve.

The integration over θ was performed graphically. For this, the quantity $(I_{tot}/I_0)\sin\theta$ was plotted versus θ (see figure 2). Since this quantity approaches zero for 0° and 180° the extrapolation to these points in the angular range not covered by the measurement is easy to perform when all the maxima have been determined experimentally. With the absolute value of Q_{tot} (Ohnemus and Jost 1979) the normalization factor c could be determined via (4). Using (1) and (3) the values of $\sigma_{ela}(\theta)$, $\sigma_{exci}(\theta)$ and $\sigma_{ion}(\theta)$ are placed on an absolute scale.

3. Apparatus

A scale drawing of the apparatus is shown in figure 3. An electron source and a Faraday cup which detects the primary current are mounted on a rotatable table at the top of the vacuum chamber. In the axis of rotation, a mercury oven produces the atomic beam. Both the oven and the Farady cup are adjustable in three dimensions. The scattered electrons are detected after passing through a stationary energy filter lens which is adjustable in the scattering plane. In the forward direction the angular range of the measurement extends down to 1° at 300 eV and 150 eV and to 2° at 100 eV. These values were chosen so that the small-angle maximum of the curve $(I_{tot}/I_0)\sin\theta$ (see figure 2) was covered by the measurement. In the backward direction the usable angular range is limited by the housing of the electron source and extends up to 165° at all energies. The Earth's magnetic field was reduced to less than 0.4 A m^{-1} in the scattering region. In addition, a mu-metal shielding (not shown in figure 3) was used for the filter lens, in which the electrons are greatly slowed.

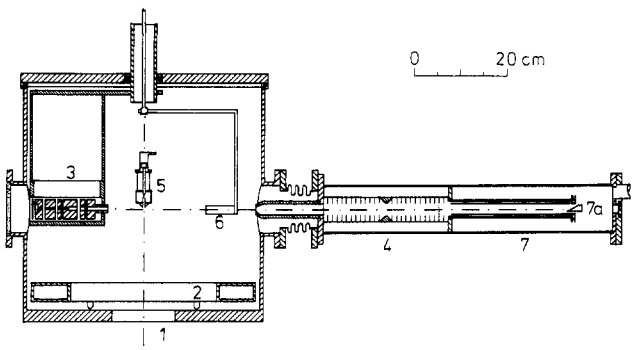

Figure 3. Vertical cross section of the apparatus (to scale). Key: 1, opening for the mercury diffusion pump; 2, cold trap; 3, rotatable electron source; 4, stationary filter lens; 5, mercury oven; 6 and 7, Faraday cups; 7a, thin wedge-shaped metal sheet.

The electron beam was generated in an electron optical lens system similar to that described by Chutjian (1979). The adjustment of the beam and its diameter could be monitored on a luminescent screen placed at a distance of 32 cm from the exit hole (diameter 1 mm) of the source. At 300 eV, the beam diameter was less than 2 mm; at 100 eV it increased to 4 mm. This yields an angular divergence of the primary beam of less than ±1°. At the smallest angles we improved our angular resolution to $\approx 0.5°$, which normally implied a lower beam intensity. The primary current was usually in the 10^{-7} A range at all energies. It was measured with a Balzers type EP 511/QME 311 electrometer. The scattering angles were varied by rotating the electron source and recorded by an angular encoder with resolution 0.02°.

The mercury beam was produced by a cylindrical oven (internal diameter 29 mm, height 27 mm) which was made of stainless steel. Its exit (length 27 mm, internal diameter 1 mm) could be closed pneumatically. The oven was DC heated using a bifilar winding of resistance wire to avoid a magnetic field. Operating temperatures of 140–150 °C were sufficient to produce scattered currents of $\geq 5 \times 10^{-16}$ A in the deepest minima of $\sigma(\theta, E)$. The oven was flanged to the vacuum chamber at a 'scattering angle' of 45° so that the electron source could not reach the angular range from 10° to 80°

on this side. The mercury oven aimed at the mercury diffusion pump, so that, with the cold trap at the bottom of the vacuum chamber, the background pressure was kept below 2×10^{-4} Pa. This is why background correction was not necessary (cf section 2). While the oven was closed, the pressure within the chamber was less than 2×10^{-5} Pa.

The scattered electrons were separated by an energy filter lens similar to that described by Zeman *et al* (1971) (middle region slightly modified) and were detected with a Faraday cup (numbered 7 in figure 3). Positive ions were suppressed by a wire mesh at + 10 V in front of the last electrode. The Faraday cup was connected to a Keithley type 642 electrometer, which recorded currents down to about 5×10^{-16} A. At the bottom of the cup the electrons were reflected onto the inner walls by a thin metal sheet (7a in figure 3) which was set to a slightly negative potential with respect to the cathode. This arrangement allowed optical adjustment of the filter lens with respect to the scattering centre. The internal diameters of the cup and the electrodes are large enough to ensure that every trajectory accepted by the aperture system in front of the filter lens ends within the cup. This was checked by a ray tracing program at each energy used. That means that the transmission of the filter lens is constant in the energy ranged. The aperture system which defines the acceptance cone consists of a circular hole (radius 2 mm) followed by a vertical slit (width 3 mm); the distance between them is $\approx$ 100 mm and the distance of the circular hole to the atomic beam is $\approx$ 250 mm. The relative energy resolution $\Delta E/E_0$ of the filter lens was 0.3%.

4. Measurement

The filter lens acts as a potential barrier of variable height. The scattered current as a function of the retarding potential gives an integral energy spectrum of the scattered electrons (see figure 4). The cut-off energy is equal to the primary energy E_0. With a retarding potential of $E_{ela} = E_0 - 2$ eV only elastically scattered electrons are able to pass the filter lens; the measured current I_{ela} is described by (1). At the end of the plateau some electrons that have excited the $6\,^3P_0$ level contribute to the scattered signal. At a retarding potential of $E_0 - E_{ion}$, where E_{ion} is the ionization energy of 10.38 eV, each electron that has excited a mercury atom and is scattered into the direction of observation contributes to the measured current $I_{ela} + I_{exci}$. By subtracting I_{ela} the current I_{exci} given in (3) could be determined.

The two electrons emerging from a single ionization process have a total energy of $E_0 - E_{ion}$ if the mercury atom is left in its ground state. The faster (scattered) electron has an energy $> \frac{1}{2}(E_0 - E_{ion})$, the slower (ejected) one has an energy $< \frac{1}{2}(E_0 - E_{ion})$. The terms of 'scattered' and 'ejected' electrons are used here in keeping with the standard literature (Mott and Massey 1971). Therefore, with a retarding potential of $\frac{1}{2}(E_0 - E_{ion})$ exactly one electron of each single-ionization process is able to pass the filter lens. Consequently, the current $I_{tot} = I_{ela} + I_{exci} + I_{ion}$ measured with this retarding potential contains the total number of electrons that were scattered by the atomic beam into the direction of observation. Electrons from multiple ionization processes may, however, possess an energy distribution that allows none of them to pass the potential barrier $\frac{1}{2}(E_0 - E_{ion})$. The error due to this effect will be discussed in section 5.

The procedure of adjusting the apparatus is described elsewhere (Fink *et al* 1975). The two (electronic and atomic) beams have to cross each other in such a way that

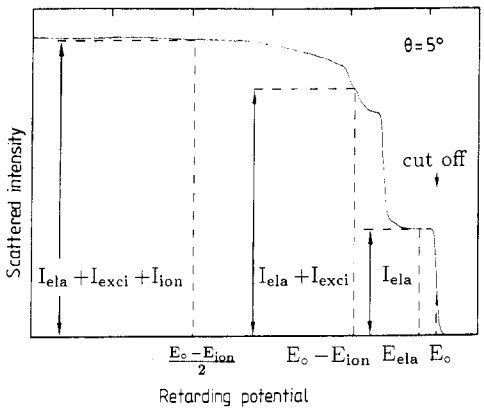

Figure 4. Intensity transmitted by the filter lens at 300 eV primary energy. This curve represents an integral spectrum of mercury. The cut-off energy E_0 is equal to the primary energy.

the crossing point lies in the axis of rotation of the electron source. Furthermore, the atomic beam has to lie within the acceptance cone of the filter lens. Both conditions were checked before a new measurement was started. The apparatus was controlled by a microcomputer which set the scattering angle and the various retarding potentials of the filter lens, opened and closed the mercury oven and collected all the data $(I_{ela}/I_0,\ (I_{ela}+I_{exci})/I_0,\ I_{tot}/I_0)$. For the primary and scattered currents 20 and 100 values, respectively, were averaged at each measuring point. There was plenty of time (2 min) between the collection of the various data to ensure stabilization of the measured quantities. Where possible (see section 3), the data were recorded for 'positive' and 'negative' scattering angles θ in order to check the symmetry of the arrangement and to determine the zero scattering angle. The cross sections given in tables 2, 3 and 4 are the arithmetic means of the two results thus obtained. The whole angular range was divided into several sections in order to take the data in the most sensitve range of the electrometer. These sections, which overlapped for at least two angles, were fitted together to evaluate the curve $(I_{tot}/I_0)\sin\theta$.

5. Experimental uncertainties

Our data contain a number of uncertainties. Considerable effort has been made to identify and quantify all the errors in the present work.

A crucial source of error in the measurement was the overlap geometry of the electron and atom beam with the detector acceptance cone (see section 2). Several experimental configurations were tried by varying the size and the distance of the aperture system to assess the effects of change in the experimental geometry. The final experimental configuration described in section 3 was one which allowed a generous margin of error in positioning the target–acceptance cone alignment.

The zero of the angular scale was determined within 0.1° by exploiting the fact that the quantity I_{ela}/I_0 has to be symmetric around $\theta = 0°$. In the angular range from 10° to 80° the accuracy of the adjustment was estimated to be only 1° because symmetric measurements were not possible (see section 3). The total angular resolution of 2° base width was caused by the primary beam spread, the diameter of the atomic beam and the aperture system. An attempt to correct the data for the angular resolution has not been made because its influence is small compared to other error sources.

The different voltage settings of the filter lens rely on the determination of the cut-off energy E_0 (see figure 4) which was carried out graphically before each measurement. This determination was accurate to within 0.1 eV. The corresponding uncertainty in the setting of E_{ela} did not influence the observed values of I_{ela} because this current was measured in the plateau of the transmitted intensity. The influence on I_{exci} and I_{tot} was $\approx 2\%$ and $\approx 0.2\%$, respectively, at small angles. At large scattering angles this influence was $\leq 0.1\%$ because of the much weaker energy dependence of the transmitted intensity in this regime.

Table 1. Rough estimate of the influence of multiple ionization on the differential cross sections (see also text). The quantity I^{n+} summarizes all ionization processes higher than double ($I_{ion} = I^+ + I^{2+} + I^{n+}$).

E_0 (eV)	$E_0 - 29.2$ (eV)	$\frac{E_0 - E_{ion}}{2}$ (eV)	$\frac{I_{ion}}{I_{tot}}$ (%)	$\frac{I^+}{I_{ion}}$ (%)	$\frac{I^{2+}}{I_{ion}}$ (%)	Fraction not discovered	$\frac{I^{n+}}{I_{ion}}$ (%)	$\frac{\sigma_{ela}}{\sigma_{exci}}$ (%)	σ_{ion} (%)
100	70.8	44.81	20	84	15	0.5	1	+2	−7
150	120.8	69.81	20	81	17	0.5	2	+2	−9
300	270.8	144.81	10	79	17	0.1	4	+1	−5

The measured differential cross sections were normalized to the absolute total cross section Q_{tot} as described in section 2. The current I_{tot}, when integrated over all angles, should contain all scattered electrons. But in our arrangement this current can be underestimated for two reasons: first, if multiple ionization occurs and second, if mercury ions are left in an excited state. Let us discuss, as an example, the influence of multiple ionization at $E_0 = 100$ eV by using the data given in table 1. The excitation threshold for double ionization is 29.2 eV (Landolt–Börnstein 1950) so that the remaining energy of 70.8 eV will be divided between the three electrons involved. The retarding potential of the filter lens for determing I_{tot} is $\frac{1}{2}(100 - 10.38) = 44.81$ eV. The current I_{ion} contributes $\approx 20\%$ to the total current I_{tot}. Single ionization processes contribute $\approx 84\%$, double ionization processes $\approx 15\%$, and all higher ionization processes $\approx 1\%$ to the current I_{ion} (Bleakney 1930). We made very roughly the assumption that 50% of the double ionization processes and 100% of the higher ionization processes lead to an energy distribution which allows none of the electrons to pass the filter lens. (At the other values of E_0 the assumption concerning the higher ionization processes was the same.) These data yield an underestimation of the normalization factor (see (4)) of $0.2 \times 0.15 \times 0.5 + 0.2 \times 0.01 = 0.017$ ($\approx 2\%$) which means that the data for $\sigma_{ela}(\theta)$ and also for $\sigma_{exci}(\theta)$ are therefore overestimated (see (1) and (3)). The values of $\sigma_{ion}(\theta)$ are underestimated by $0.15 \times 0.5 + 0.01 = 0.085$ ($\approx 9\%$) and must also be corrected by the $\approx 2\%$ of the normalization factor which results in an underestimation of $\approx 7\%$. The corresponding corrections for $E_0 = 150$ and 300 eV are also listed in table 1. The contribution of ionization processes where the mercury ion is not left in its ground

state is not exactly known. Measurements on noble gases (Varga and Winter 1978) show, however, that they contribute $\approx 2\%$ to all ionization processes. Besides, some of the electrons emerging from such processes can pass the filter lens so that the overall influence on the differential cross section is assumed to be less than 1%.

Multiple scattering was checked by measuring the ratio $I_{tot}(\theta)/I_{ela}(\theta)$ at different target densities (i.e. at different oven temperatures in the range from 165 °C to 140 °C) and at different scattering angles. This ratio varies outside the regime of single scattering because I_{ela} and I_{tot} are affected by multiple scattering in a different way. But no effect was found in the temperature range mentioned. Nevertheless, we used the lowest temperature which was sufficient to produce measurable scattered currents. Variations of the oven temperature by ±2 °C lead at most to a change of the target density of less than 5% (Nesmeyanov 1963). The zero drift of the electrometer was $\leq 3 \times 10^{-17}$ A which is noticeable only at the deepest minima of the cross sections where it results in an uncertainty of 5%. The total cross section Q_{tot} is known within 15% and the uncertainty of the graphic integration was 1% at all energies.

The total uncertainties $\Delta\sigma$ given in tables 2, 3 and 4 were obtained by adding the aforementioned contributions quadratically, i.e. assuming that they are uncorrelated. This yields an uncertainty of 16% for $\sigma_{ela}(\theta)$. For the quantities $\sigma_{exci}(\theta)$ and $\sigma_{ion}(\theta)$ the uncertainty can rise up to 50% and 25%, respectively, because these cross sections were obtained by subtraction of two measured currents.

Table 2. Absolute elastic differential cross sections $\sigma_{ela}(\theta)$ and absolute uncertainties $\Delta\sigma$ for electron–mercury scattering (in units of a_0^2 sr^{-1}).

	$E_0 = 100$ eV		$E_0 = 150$ eV		$E_0 = 300$ eV	
θ (deg)	$\sigma_{ela}(\theta)$	$\Delta\sigma$	$\sigma_{ela}(\theta)$	$\Delta\sigma$	$\sigma_{ela}(\theta)$	$\Delta\sigma$
1			253.5	40.6	221.3	35.4
2	215.7	34.5	188.3	30.1	172.9	27.7
3	178.2	28.5	158.4	25.3	149.2	23.9
4	148.2	23.7	133.5	21.4	125.9	20.1
110	0.243	0.039	0.006	0.001	0.120	0.019
112			0.007	0.001		
114			0.009	0.002		
115	0.146	0.023			0.040	0.008
116			0.019	0.003		
120	0.077	0.012	0.040	0.007	0.009	0.002
125	0.030	0.005	0.077	0.012	0.019	0.004
128	0.020	0.004				
130	0.018	0.003	0.109	0.017	0.047	0.008
133	0.023	0.004			0.055	0.009
135	0.031	0.005	0.124	0.020	0.055	0.009
137					0.053	0.009
138	0.043	0.008	0.122	0.020		
140	0.060	0.010	0.119	0.019	0.040	0.008
142			0.111	0.017	0.029	0.006
145	0.094	0.016	0.097	0.016	0.017	0.003
148					0.014	0.003
150	0.154	0.025	0.057	0.009	0.023	0.005
155	0.221	0.035	0.025	0.005	0.094	0.015
160	0.292	0.047	0.007	0.002	0.253	0.041
165	0.322	0.052	0.002	0.001	0.299	0.049

6. Results and discussion

6.1. Elastic differential cross sections

The elastic differential cross sections obtained with the present crossed beam method are shown in figure 5 together with the data of Holtkamp *et al* (1987) obtained with a static gas target. Our data are listed in table 2 except for those angular ranges where reliable results were already given in the latter paper. For comparison with other experimental and theoretical data we refer to that paper, too. At 300 eV, our results are seen to be slightly higher whereas at 100 and 150 eV they are in general somewhat lower than those of Holtkamp *et al* (1987). In general, agreement between the two data sets is given within their combined uncertainties. Especially at small scattering angles where, with the static gas target, the correction for changes of the scattering volume becomes complicated (see section 1) we find agreement at all energies. Discrepancies exist, however, at 100 and 150 eV at scattering angles $\geq 110°$ where our data are lower and somewhat outside the combined errors. A clear-cut reason for this cannot be given; we assume, however, that it is related to our findings at 50 eV, where the agreement within the combined uncertainties was confined to angles $\leq 55°$. At this

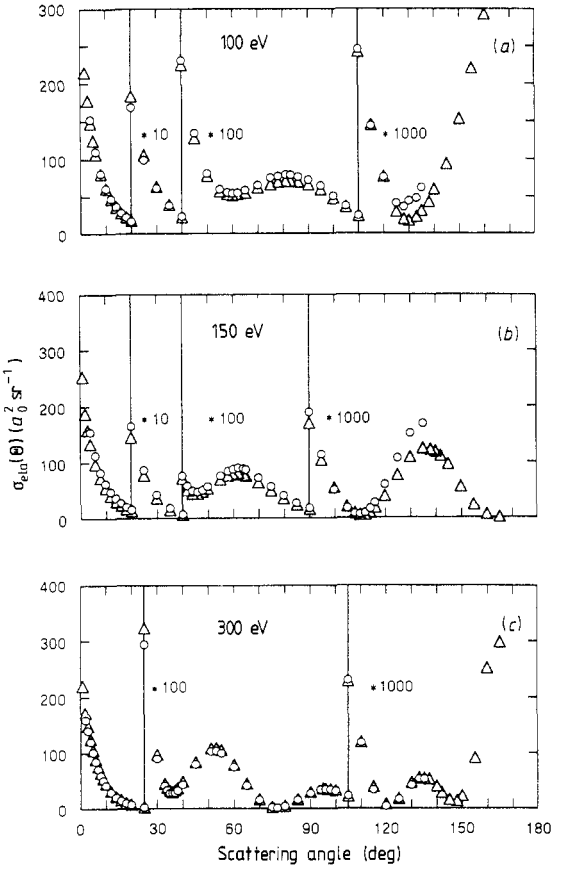

Figure 5. Absolute differential cross sections for elastic electron scattering from mercury. (*a*) 100 eV, (*b*) 150 eV, (*c*) 300 eV. Δ, this work; O, data of Holtkamp *et al* (1987) obtained with a static gas target.

energy, our method requires detection of electrons down to ≈ 20 eV, so that residual electric and magnetic fields over an electron path length of ≈ 70 cm may influence this measurement in an unknown manner.

6.2. Differential excitation and ionization cross sections

The results for differential excitation and ionization cross sections are presented in figure 6 and listed in tables 3 and 4. Other experimental and theoretical data do not exist. The ionization cross section $\sigma_{ion}(\theta)$ measured in the present experiment describes the angular distribution of the electrons that were scattered during the ionization process in the sense defined in section 4. The shapes of the curves are not as smooth as in the elastic case, because the data were obtained by subtraction of measured currents which results in higher statistical uncertainties (see section 5). But it is obvious that the shape of $\sigma_{exci}(\theta)$ is similar to that of $\sigma_{ela}(\theta)$, a fact which supports a two-step model of the excitation process (Massey and Burhop 1969). Such a similarity in shape is not found in $\sigma_{ion}(\theta)$. In the energy range covered by our measurements the excitation cross sections are strongly peaked in the forward direction. This is shown for 300 eV in figure 7 where the elastic and excitation cross sections are compared with each other. At this energy, approximately 90% of the electrons

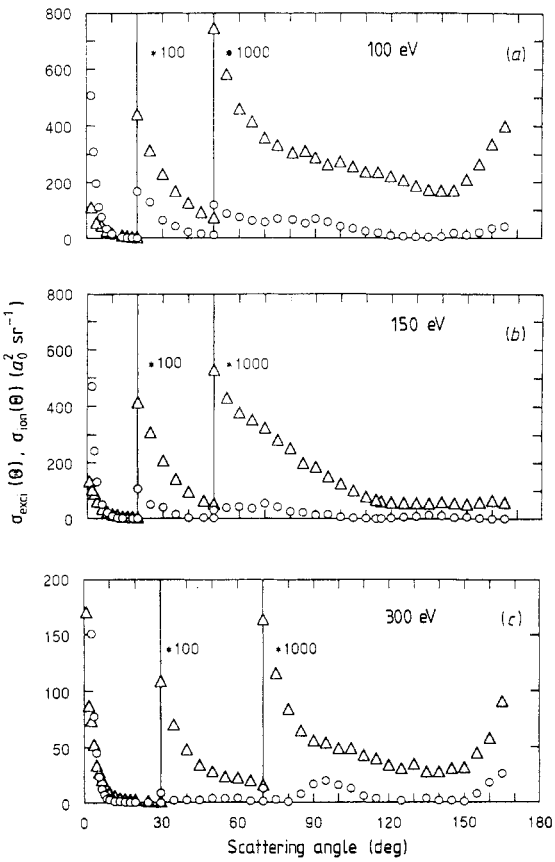

Figure 6. Absolute differential excitation and ionization cross sections for electron impact of mercury. (*a*) 100 eV, (*b*) 150 eV, (*c*) 300 eV. Δ, ionization; O, excitation.

Table 3. Absolute differential excitation cross sections $\sigma_{exci}(\theta)$ and absolute uncertainties $\Delta\sigma$ for electron–mercury scattering (in units of a_0^2 sr^{-1}).

	$E_0 = 100$ eV		$E_0 = 150$ eV		$E_0 = 300$ eV	
θ (deg)	$\sigma_{exci}(\theta)$	$\Delta\sigma$	$\sigma_{exci}(\theta)$	$\Delta\sigma$	$\sigma_{exci}(\theta)$	$\Delta\sigma$
2	508	81	470	80	334	57
4	197	32	132	22	77.7	13
6	77.0	13	51.3	8.7	23.5	4.0
8	34.5	5.6	22.0	3.8	7.4	1.3
10	17.0	2.8	10.1	1.7	3.0	0.5
12			2.9	0.7	1.5	0.3
14	4.4	1.0	2.1	0.7	1.3	0.2
16	1.8	0.8	1.0	0.4	0.92	0.16
18	1.8	0.7	1.6	0.4	0.68	0.11
20	1.7	0.3	1.1	0.2	0.55	0.09
25	1.3	0.2	0.51	0.14	0.21	0.04
30	0.65	0.14	0.41	0.11	0.088	0.015
35	0.43	0.12	0.17	0.04	0.022	0.004
40	0.23	0.08	0.040	0.014	0.024	0.004
45	0.17	0.03			0.024	0.004
50	0.12	0.02	0.031	0.018	0.039	0.007
55	0.088	0.018	0.040	0.017	0.039	0.007
60	0.076	0.013	0.043	0.020	0.042	0.007
65	0.063	0.016	0.038	0.014	0.016	0.003
70	0.058	0.011	0.056	0.016	0.013	0.002
75	0.069	0.024	0.043	0.012	0.003	0.001
80			0.027	0.008	0.001	0.001
85			0.023	0.006	0.008	0.002
90	0.070	0.024	0.014	0.002	0.017	0.003
95	0.058	0.018	0.017	0.003	0.020	0.004
100	0.049	0.011	0.008	0.002	0.016	0.003
105	0.036	0.010	0.004	0.002	0.013	0.002
110	0.025	0.007	0.003	0.001	0.006	0.002
115	0.020	0.004			0.004	0.002
120	0.010	0.003	0.004	0.002		
125	0.008	0.002	0.008	0.002		
130	0.006	0.001	0.010	0.003		
135	0.004	0.001	0.014	0.004	0.004	0.002
140	0.007	0.002	0.012	0.004	0.002	0.001
145	0.019	0.004	0.006	0.002	0.002	0.001
150	0.012	0.004	0.008	0.002	0.001	0.001
155	0.021	0.005	0.003	0.001	0.008	0.002
160	0.035	0.008	0.001	0.001	0.018	0.003
165	0.042	0.008	0.002	0.001	0.026	0.005

that have excited the mercury atom are found between 0° and 10°, while for elastic scattering the corresponding value is 40%.

6.3. Angle-integrated cross sections

By graphic integration and normalization to Q_{tot}, as described in section 2, the angle-integrated cross sections for elastic scattering (Q_{ela}), for excitation (Q_{exci}) and for ionization (Q_{ion}) were obtained. The results are listed in table 5 together with the values for Q_{tot} of Ohnemus and Jost (1979). The values for Q_{ela} agree within the combined errors with those of Holtkamp *et al* (1987). This also holds true for Q_{exci},

Table 4. Absolute differential ionization cross sections $\sigma_{ion}(\theta)$ and absolute uncertainties $\Delta\sigma$ for electron–mercury scattering (in units of a_0^2 sr^{-1}).

	E_0 = 100 eV		E_0 = 150 eV		E_0 = 300 eV	
θ (deg)	$\sigma_{ion}(\theta)$	$\Delta\sigma$	$\sigma_{ion}(\theta)$	$\Delta\sigma$	$\sigma_{ion}(\theta)$	$\Delta\sigma$
2	112	19	105	18	87.4	15
4	56.6	9.6	61.6	12	52.6	8.9
6	46.2	7.9	36.5	6.1	27.7	4.7
8	27.2	4.9	24.5	4.0	17.3	2.9
10	19.4	3.2	15.5	2.6	9.8	1.7
12			13.3	2.2	6.5	1.1
14	10.0	1.7	8.2	1.6	4.2	0.7
16	8.2	1.5	6.6	1.2	3.4	0.6
18	5.4	1.1	5.2	0.9	2.9	0.5
20	4.4	0.7	4.1	0.7	2.4	0.4
25	3.1	0.5	3.1	0.5	1.7	0.3
30	2.3	0.4	2.1	0.4	1.1	0.2
35	1.7	0.3	1.4	0.2	0.70	0.12
40	1.3	0.2	0.97	0.16	0.48	0.08
45	0.93	0.15			0.34	0.06
50	0.75	0.12	0.53	0.09	0.28	0.05
55	0.58	0.09	0.43	0.07	0.24	0.04
60	0.46	0.08	0.38	0.06	0.23	0.04
65	0.42	0.07	0.35	0.06	0.20	0.03
70	0.36	0.06	0.33	0.05	0.16	0.03
75	0.33	0.06	0.28	0.05	0.12	0.02
80			0.25	0.04	0.084	0.014
85			0.20	0.03	0.065	0.011
90	0.29	0.05	0.19	0.03	0.056	0.009
95	0.26	0.05	0.15	0.02	0.054	0.009
100	0.27	0.05	0.13	0.02	0.049	0.008
105	0.26	0.05	0.10	0.02	0.049	0.008
110	0.24	0.04	0.08	0.01	0.043	0.007
115	0.24	0.04			0.040	0.007
120	0.22	0.04	0.06	0.01	0.034	0.006
125	0.21	0.03	0.06	0.01	0.031	0.005
130	0.19	0.03	0.06	0.01	0.035	0.005
135	0.17	0.03	0.06	0.01	0.028	0.005
140	0.17	0.03	0.06	0.01	0.028	0.005
145	0.17	0.03	0.06	0.01	0.031	0.005
150	0.21	0.03	0.05	0.01	0.032	0.005
155	0.27	0.04	0.06	0.01	0.045	0.008
160	0.34	0.06	0.07	0.02	0.058	0.010
165	0.40	0.07	0.06	0.01	0.091	0.015

although this quantity was estimated empirically by Holtkamp *et al* (1987) from the data of Ohnemus and Jost (1979) for Q_{tot} and an earlier measurement of Smith (1931) for Q_{ion}. Since Smith (1931) does not indicate the accuracy of his data, Holtkamp *et al* (1987) assigned—rather arbitrarily—an error of 20% to Smith's results. Our data for Q_{ion} agree with those of Smith (1931) as modified by Holtkamp *et al* (1987) within the combined uncertainties except for 300 eV.

Our measurements show that the relative contributions of Q_{ela} ($\approx$60%), Q_{exci} ($\approx$20%) and Q_{ion} ($\approx$20%) to Q_{tot} are roughly the same at 100, 150 and 300 eV. At 100 eV, the global quantity Q_{exci} can be further disentangled because the angle-

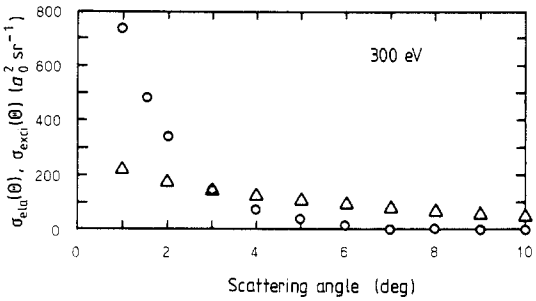

Figure 7. Absolute differential cross sections at 300 eV for mercury at small scattering angles. Δ, elastic; O, excitation.

Table 5. Absolute total and angle-integrated cross sections together with absolute uncertainties Δ Q for electron–mercury scattering (in units of a_0^2).

	Q_{tot}		Q_{ela}		Q_{exci}		Q_{ion}	
	Q	ΔQ	Q	ΔQ	Q	ΔQ	Q	ΔQ
100 eV	59.0	8.9	31.8	4.8	13.2	2.1	14.0	2.8
150 eV	45.7	6.9	24.9	3.7	10.2	1.6	10.6	2.1
300 eV	31.3	4.7	19.1	2.9	6.3	1.0	5.9	1.1

integrated cross section for 6^1P_1 excitation has been separately found to be $(10.8 \pm 3)\ a_0^2$ (Peitzmann and Kessler 1990). All other inelastic (non-ionizing) channels should therefore contribute $(13.2 \pm 2.1)\ a_0^2 - (10.8 \pm 3.0)\ a_0^2 = (2.4 \pm 5.1)\ a_0^2$ to Q_{exci} which is a fraction of the order of 20%. This is consistent with the findings of Ohnemus and Jost (1979) who estimated this contribution to be $\approx$ 10% at 300 eV.

7. Conclusion

It was the purpose of the present paper to check the consistency of the absolute elastic cross sections that have been measured by two different methods which both have their strengths and their weaknesses. The main advantage of the crossed beam technique used here is that the scattering volume is independent of the scattering angle. The agreement of the present data with those obtained earlier with the static gas technique proves the reliability of the corrections for the effective path length that are necessary when using that technique. The agreement is good, in particular at small scattering angles where the corrections for the effective path length are crucial. The consistency of the two sets of absolute elastic differential cross sections is a stringent test for their reliability. Such a consistency check seemed quite important to us, since one frequently finds discrepancies between the absolute cross sections measured by different groups or methods that are larger than the error limits claimed by the authors (Kessler 1986).

Comparing the two methods discussed here we consider, in general, the static gas technique to be superior because of two reasons: first of all, it yields absolute cross sections for each scattering angle directly (i.e. without normalization procedure).

Second, it avoids an error source that is typical of the method described here: it does not have to cope with multiple ionization processes and the uncertainties caused by them. Nevertheless, the atomic beam method yields absolute differential cross sections with a reliability of roughly 20%, a value which can be reduced by a more accurate measurement of Q_{tot}.

From the present measurements we could also derive differential cross sections for excitation and ionization, which have hitherto not been available.

Acknowledgments

We are grateful for the cooperation of the late Dr K Jost whose ideas and achievements have considerably influenced this work. Support by the Sonderforschungsbereich 216 of the Deutsche Forschungsgemeinschaft is gratefully acknowledged.

References

Bleakney W 1930 *Phys. Rev.* **35** 139
Bromberg J P 1969 *J. Chem. Phys.* **51** 4117
Chutjian A 1979 *Rev. Sci. Instrum.* **50** 347
Fink M, Jost K and Herrman D 1975 *Phys. Rev.* A **12** 1374
Holtkamp G, Jost K, Peitzmann F J and Kessler J 1987 *J. Phys. B: At. Mol. Phys.* **20** 4543
Kessler J 1986 *Comment. At. Mol. Phys.* **18** 279
Landolt–Börnstein 1950 *Zahlenwerte und Funktionen* 6th edn 1 Band, 1 Teil (Berlin: Springer)
Massey H S W and Burhop E H S 1969 *Electronic and Ionic Impact Phenomena I* 2nd edn (Oxford: Clarendon) ch 8.7.2
Mott N F and Massey H S W 1971 *The Theory of Atomic Collisions* 3rd edn (Oxford: Clarendon) ch 16, sec 8.3
Nesmeyanov A 1963 *Vapour Pressure of the Chemical Elements* (Amsterdam: Elsevier)
Ohnemus B and Jost K 1979 *Phys. Rev.* A **19** 641
Peitzmann F J and Kessler J 1990 *J. Phys. B: At. Mol. Opt. Phys.* **23** 2629
Silverstein E A 1959 *Nucl. Instrum. Methods* **4** 53
Smith P 1931 *Phys Rev.* **37** 808
Shyn T W, Stolarski R S and Carignan G R 1972 *Phys. Rev.* A **6** 1002
Varga P and Winter H 1978 *Phys. Rev.* A **18** 2453
Zeman H D, Jost K and Gilad S 1971 *Rev. Sci. Instrum.* **42** 485